J. Phys.: Condens. Matter **20** (2008) 395006 (11pp) doi:10.1088/0953-8984/20/39/395006

On the origin of Amonton's friction law

B N J Persson[1,2], I M Sivebaek[1,3,4], V N Samoilov[1,5], Ke Zhao[6], A I Volokitin[1,7] and Zhenyu Zhang[2,6]

[1] IFF, FZ-Jülich, D-52425 Jülich, Germany
[2] Materials Science and Technology Division, Oak Ridge National Laboratory, Oak Ridge, TN 37831, USA
[3] Novo Nordisk A/S, Research and Development, DK-3400 Hillerod, Denmark
[4] Mechanical Engineering Department, Technical University of Denmark, DK-2800 Lyngby, Denmark
[5] Physics Faculty, Moscow State University, 117234 Moscow, Russia
[6] Department of Physics and Astronomy, University of Tennessee, Knoxville, TN 37996-1200, USA
[7] Physical Department, Samara State Technical University, 443100 Samara, Russia

Received 16 June 2008, in final form 13 August 2008
Published 4 September 2008
Online at stacks.iop.org/JPhysCM/20/395006

Abstract

Amonton's law states that the sliding friction force increases linearly with the load. We show that this result is expected for stiff enough solids, even when the adhesional interaction between the solids is included in the analysis. As a function of the magnitude of the elastic modulus E, one can distinguish between three regions: (a) for $E > E_2$, the area of real contact (and the friction force) depends linearly on the load, (b) for $E_1 < E < E_2$, the area of real contact depends nonlinearly on the load but vanishes for zero load, and (c) for $E < E_1$ the area of real contact depends nonlinearly on the load and is non-vanishing at zero load. In this last case a finite pull-off force is necessary in order to separate the solids. Based on molecular dynamics calculations, we also discuss the pressure dependence of the frictional shear stress for polymers. We show that the frictional shear stress is independent of the normal pressure p_0 as long as p_0 is much smaller than the adhesional pressure $p_{\rm ad}$, which depends on the atomic corrugation of the solid surfaces in the sliding interface. Finally, we discuss the origin of why the contact area between a soft elastic solid (e.g. rubber) and a flat substrate decreases from the JKR (adhesive contact) limit at zero or small sliding velocities, to the Hertz (non-adhesive) limit at high sliding velocities.

(Some figures in this article are in colour only in the electronic version)

1. Introduction

Sliding friction represents a highly complex topic of great practical importance [1]. For many sliding systems it is found that the friction force $F_{\rm f}$ is proportional to the load or normal force $F_{\rm N}$ (see [2, 3]), i.e.

$$F_{\rm f} = \mu F_{\rm N}.$$

This friction 'law' is usually explained by assuming that, because of the surface roughness, which exists on nearly all solid surfaces, the area of real (atomic) contact is proportional to the load [3], i.e.

$$A = \alpha F_{\rm N}$$

and the stress (or pressure) distribution in the contact areas is *independent* of the load. The friction force can then be written as

$$F_{\rm f} = \sigma_{\rm f} A = \sigma_{\rm f} \alpha F_{\rm N}$$

where $\sigma_{\rm f}$ is the (average) frictional shear stress in the area of real contact. Note that, even if the frictional shear stress $\sigma_{\rm f}$ depends on the local pressure in the contact area, as long as this pressure distribution is independent of the load, the friction will not depend on the detailed pressure distribution in the contact areas or on the pressure dependence of $\sigma_{\rm f}$, and $\mu = \sigma_{\rm f}\alpha$ will be independent of the load [4]. This is usually true even for viscoelastic solids such as rubber sliding on hard rough substrates, where the friction is determined not just by

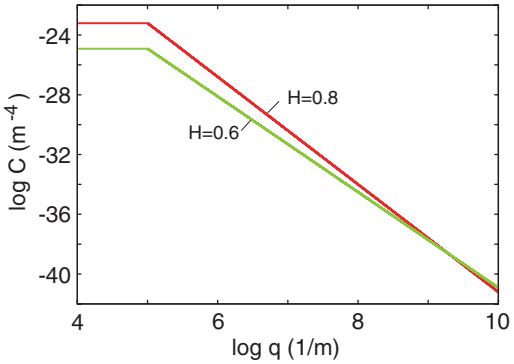

Figure 1. The logarithm (with 10 as the base) of the surface roughness power spectrum $C(q)$ as a function of the logarithm of the wavevector for two self-affine fractal surfaces with the Hurst exponent $H = 0.8$ and 0.6. Both surfaces have the same surface area $\approx 1.37 A_0$ (where A_0 is the nominal contact area) but the root-mean-square roughness differs: $h_{\rm rms} = 0.66\ \mu$m and $1.01\ \mu$m for the surfaces with $H = 0.6$ and 0.8, respectively.

the area of real contact, but it depends on the deformation of the rubber on all length scales [5][8].

It has been suggested that the origin of Amonton's law is an approximately linear dependence of the frictional shear stress on the normal stress [6]. However, a linear dependence is not always observed in computer simulations, and in any case, as mentioned above, the actual dependence of the frictional shear stress on the normal stress or pressure is irrelevant in most cases when surfaces roughness occur on many different length scales.

The assumption that the area of real contact is proportional to the load is usually explained by assuming that plastic flow occurs in the asperity contact regions so that the pressure in the contact regions is determined by the indentation hardness of the solids. However, for very smooth surfaces, or for soft elastic solids such as rubber or gelatin, it is unlikely that the local pressure in the asperity contact regions reaches the penetration hardness or rupture stress. In these cases one expects purely elastic deformation to occur everywhere and it is then nontrivial to understand why the area of contact is proportional to the load since the contact area between a single spherical bump asperity and a flat surface is (in the absence of adhesion) given by the Hertz formula and depends nonlinearly on the load as $A \propto F_{\rm N}^{2/3}$. However, even in these cases it has been shown that for non-adhesive interaction between randomly rough surfaces, $A \propto F_{\rm N}$ (see appendix A). In this paper we will show that the same result holds in most cases *even when the adhesive interaction between the solids is included in the analysis*. Based on molecular dynamics calculations, we also discuss the pressure dependence of the frictional shear stress. We show that the frictional shear stress is independent of the normal pressure p_0 as long as p_0 is much smaller than the adhesional pressure $p_{\rm ad}$, which depends on the atomic corrugation of the sliding interface. Finally, we discuss the origin of why the contact area between a soft elastic solid (e.g. rubber) and a flat substrate decreases from the JKR (adhesive contact) limit at zero or small sliding velocities to the Hertz (non-adhesive) limit at high enough sliding velocities.

[8] When a rubber block is sliding on a hard, rough substrate, the substrate asperities will give rise to time-dependent deformations of the rubber surface which will result in transfer of translational energy into heat via the internal friction of the rubber. For surfaces with roughness on many length scales, it is necessary to add the energy dissipation which results from the asperities on all length scales. With respect to the most long-wavelength roughness the rubber may appear to be in complete contact with the substrate but at higher magnification, where shorter-wavelength roughness is observed, the relative contact area A/A_0 (where A_0 is the nominal contact area) is usually much smaller than unity. When $A/A_0 \ll 1$ the contact area is proportional to the load, and since the short-wavelength roughness (where $A/A_0 \ll 1$) usually gives the dominant contribution to the rubber friction, one expects the friction force to be (nearly) proportional to the load $F_{\rm N}$. In real situations this proportionality is not always observed, but the reason for this is usually due to other effects, such as frictional heating which depends on the load. Rubber friction theories (such as [5]) built on the Greenwood–Williamson contact mechanics theory do find a load dependence of the rubber friction, but in our opinion this is due to the failure of the Greenwood–Williamson theory to describe correctly the contact mechanics when roughness occurs on many different length scales (see appendix A and [26]).

2. Contact mechanics for randomly rough (self-affine fractal) surfaces

We will study the contact between a hard, randomly rough substrate and an elastic solid with a flat surface. We consider two rough self-affine fractal surfaces with the fractal dimensions $D_{\rm f} = 2.2$ and 2.4, corresponding to the Hurst exponents ($H = 3 - D_{\rm f}$) $H = 0.8$ and 0.6, respectively. The power spectra $C(q)$ (as a function of the wavevector q) of the two surfaces are shown in figure 1. Both surfaces have the surface area $\approx 1.37 A_0$ (where A_0 is the nominal or apparent contact area), but the root-mean-square roughness differs: $h_{\rm rms} = 0.66\ \mu$m and $1.01\ \mu$m for the surfaces with $H = 0.6$ and 0.8, respectively. We will present results both with and without adhesion. For the calculations with adhesion we assume that the interfacial binding energy (per unit surface area) between flat surfaces $\Delta\gamma = \gamma_1 + \gamma_2 - \gamma_{12} = 0.05$ J m^{-2}, as is typical for solids which interact (mainly) by the van der Waals interaction.

We use the theory developed in [7] to calculate how the area of real contact A depends on the applied pressure p_0 and the magnification ζ. Here the magnification $\zeta = L/\lambda$ where L is some reference length which could be the linear size of the system, and λ the resolution, i.e. the wavelength of the shortest roughness component included in the analysis. We also study how the effective interfacial binding energy (per unit nominal surface area) $\gamma_{\rm eff}(\zeta)$ depends on the magnification. Note that the pull-off force (the force necessary to separate the two solid bodies) will be non-vanishing only if the *macroscopic* interfacial binding energy $\gamma_{\rm eff}(1)$ is non-zero.

The theory of adhesion presented in [7] is based on a study of how the effective interfacial energy $\gamma_{\rm eff}(\zeta)$ and the stress distribution at the block–substrate interface depends on the magnification ζ. The effective interfacial energy is given by

$$\gamma_{\rm eff}(\zeta) A^*(\zeta) = \Delta\gamma A^*(\zeta_1) - U_{\rm el},$$

where $A^*(\zeta)$ is the contact area when the interface is studied at the magnification ζ, which in general is larger than the contact area $A(\zeta)$ projected on the xy plane. $A^*(\zeta_1)$ is the contact area

at the highest (atomic) resolution ζ_1 and $\Delta\gamma = \gamma_1 + \gamma_2 - \gamma_{12}$ is the change in the interfacial energy (per unit area) as the two solids with flat surfaces are brought together. The elastic energy stored in the asperity contact regions is denoted by $U_{\rm el}$. The physical origin of the equation above is that the effective interfacial free energy $\gamma_{\rm eff}(\zeta)A^*(\zeta)$ is equal to the free energy associated with the bonding between the two solids in the area of real contact, $\Delta\gamma A^*(\zeta_1)$, minus the stored elastic energy $U_{\rm el}$, which is given back during pull-off, thus helping to break the wall–wall atomic bonds in the area of real contact.

We assume first that the elastic modulus $E = 15$ MPa and the substrate surface has the power spectra shown in figure 1 with the Hurst exponent $H = 0.8$. In figure 2(a) we show the area of real contact A (projected on the xy plane) at the highest magnification ζ_1 (in units of the nominal contact area A_0) as a function of the nominal squeezing pressure. Figures 2(b) and (c) show the area of real contact $A(\zeta)$ and the effective interfacial binding energy (per unit surface area) (in units of $\Delta\gamma$) as a function of the magnification ζ. Results are shown both without adhesion and with adhesion using $\Delta\gamma = 0.05$ J m^{-2}. Note that in this case the area of real (atomic) contact depends linearly on the squeezing pressure p_0 (which is proportional to the load or normal force $F_{\rm N}$, $p_0 = F_{\rm N}/A_0$), while the macroscopic interfacial binding energy vanishes. We have performed a large set of similar calculations for other values of the elastic modulus and observed the same behavior as in figure 2 as long as $E > E_2 \approx 10$ MPa.

For $E < E_1 \approx 5$ MPa we find instead that the macroscopic interfacial energy and the area of real contact at zero load are both non-vanishing. This is illustrated in figure 3 when the elastic modulus $E = 3$ MPa. For $E_1 < E < E_2$ the macroscopic interfacial energy and the area of real contact at zero load are both vanishing but the area of real contact depends nonlinearly on the pressure p_0 for the (nominal) pressures $0 < p_0 < 0.1$ MPa we study (see figure 4).

We have observed the same general behavior as described above for other self-affine fractal surfaces. As an illustration, in figure 5 we show results for a surface with the fractal dimension $D_{\rm f} = 2.4$ with the power spectrum given in figure 1. This surface has the same total area as the surface with $D_{\rm f} = 2.2$, but since the roughness at short wavelengths increases and the roughness at long wavelengths decreases when the fractal dimension increases (at a constant total surface area), the adhesional interaction will be much stronger for the surface with $D_{\rm f} = 2.4$. Indeed, for $D_{\rm f} = 2.4$ the (projected) contact area (at zero load) $A \approx 0.95A_0$ when the modulus $E \approx 50$ MPa, while for the surface with $D_{\rm f} = 2.2$ the same contact area is obtained for a much softer elastic solid, when the modulus $E \approx 1$ MPa.

Figure 5 shows results for the fractal dimension $D_{\rm f} = 2.4$ and the elastic modulus $E = 120$ MPa. The area of real contact ((a) and (b)), and the effective interfacial binding energy (per unit surface area) (c) exhibit the same general behavior as when the fractal dimension $D_{\rm f} = 2.2$ and $E = 15$ MPa (see figure 2).

The results obtained above are summarized in figure 6 which shows (schematically) the relation between the area of real contact $A(\zeta_1)$ and the normal pressure $p_0 = F_{\rm N}/A_0$, as a function of the elastic modulus. In the figure 'nonlinear'

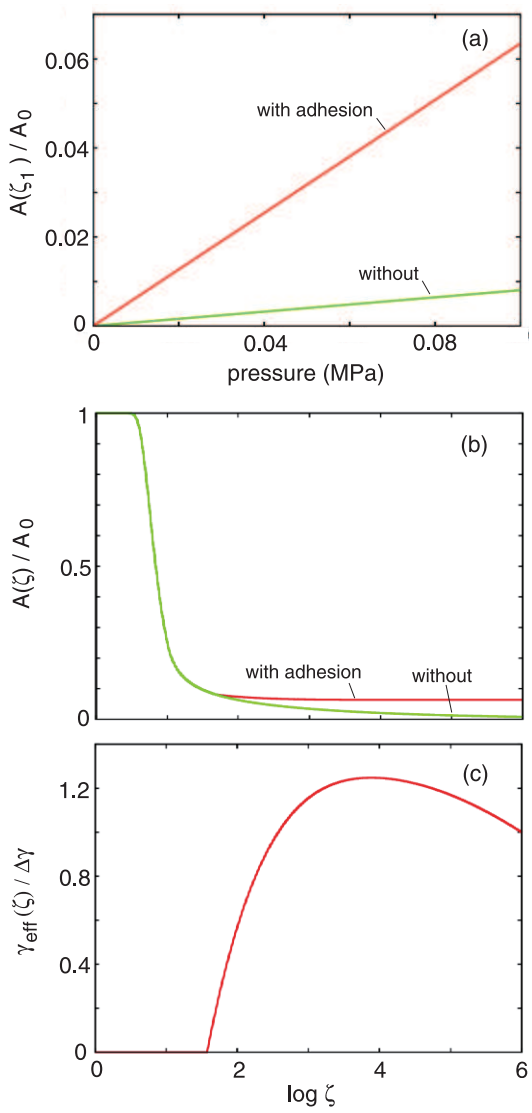

Figure 2. (a) The area of real contact A (in units of the nominal contact area A_0) at the highest magnification ζ_1 (=10^6) as a function of the nominal squeezing pressure. (b) The area of real contact $A(\zeta)$ (for the pressure $p = 0.1$ MPa) and (c) the effective interfacial binding energy (per unit surface area) (in units of $\Delta\gamma = \gamma_1 + \gamma_2 - \gamma_{12}$) as a function of the logarithm (with 10 as the base) of the magnification ζ. Results are shown both without adhesion and with adhesion using $\Delta\gamma = 0.05$ J m^{-2}. For the elastic modulus $E = 15$ MPa and the surface with the power spectrum shown in figure 1 with the Hurst exponent $H = 0.8$.

refer to the fact that the area of contact depends nonlinearly on the squeezing pressure in the pressure range *studied above*. If the studied pressure range is made smaller an (approximate) linearity may be observed between A and p_0. In general, as long as the increase in the contact area is less than ∼10% of the nominal contact area, the relation between A and p_0 will be approximately linear.

In figure 7 we show the ratio $\alpha_{\rm ad}/\alpha$ between the slopes of the relation (in the linear region) between the contact area A and the applied normal force $F_{\rm N}$ with the adhesional interaction included ($\alpha_{\rm ad}$) and without the adhesional interaction (α). We show results for the self-affine fractal surfaces (with the Hurst

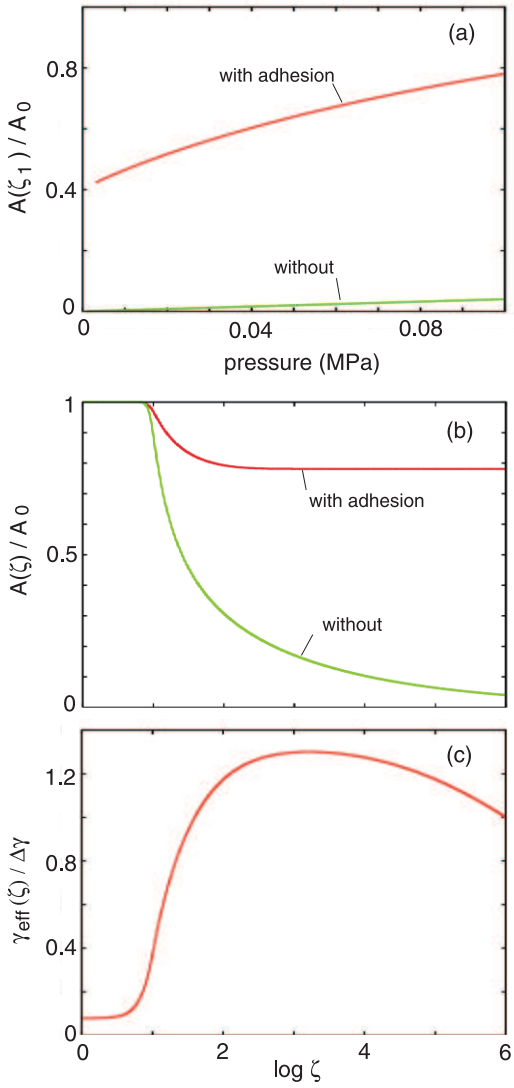

Figure 3. (a) The area of real contact A (in units of the nominal contact area A_0) at the highest magnification ζ_1 ($=10^6$) as a function of the nominal squeezing pressure. (b) The area of real contact $A(\zeta)$ (for the pressure $p = 0.1$ MPa) and (c) the effective interfacial binding energy (per unit surface area) (in units of $\Delta\gamma = \gamma_1 + \gamma_2 - \gamma_{12}$) as a function of the logarithm (with 10 as the base) of the magnification ζ. Results are shown both with and without adhesion. For the elastic modulus $E = 3$ MPa and the surface with the power spectrum shown in figure 1 with the Hurst exponent $H = 0.8$.

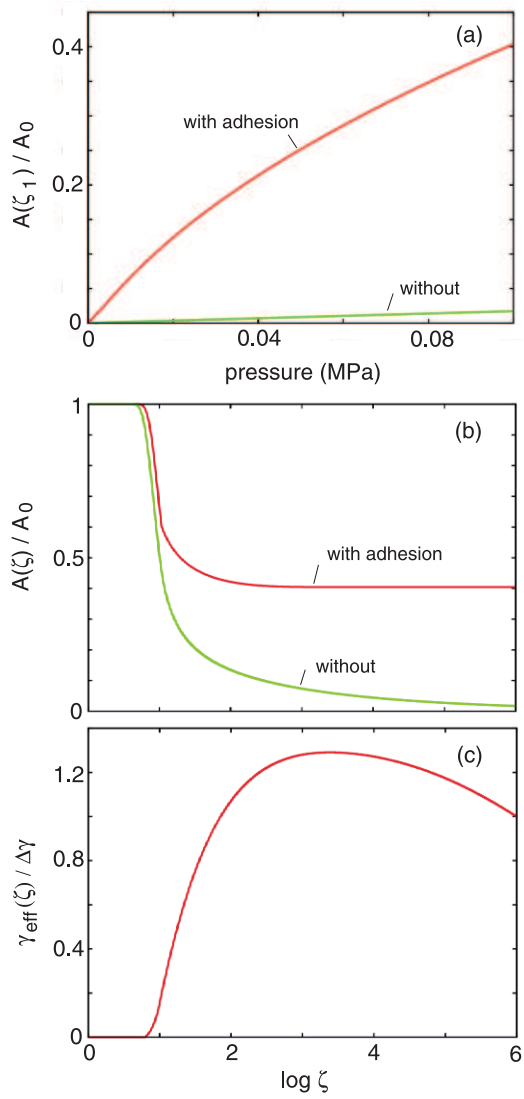

Figure 4. (a) The area of real contact A (in units of the nominal contact area A_0) at the highest magnification ζ_1($=10^6$) as a function of the nominal squeezing pressure. (b) The area of real contact $A(\zeta)$ (for the pressure $p = 0.1$ MPa) and (c) the effective interfacial binding energy (per unit surface area) (in units of $\Delta\gamma = \gamma_1 + \gamma_2 - \gamma_{12}$) as a function of the logarithm (with 10 as the base) of the magnification ζ. Results are shown both with and without adhesion. For the elastic modulus $E = 7$ MPa and the surface with the power spectrum shown in figure 1 with the Hurst exponent $H = 0.8$.

exponent $H = 0.6$ and 0.8) with the power spectra shown in figure 1.

We may state qualitatively that, when decreasing the magnification ζ, if $\gamma_{\rm eff}(\zeta)$ vanishes before reaching the macroscopic scale ($\zeta = 1$), the contact mechanics at the macroscopic scale will appear elastic and non-adhesive, and the contact area will be proportional to the load as expected for elastic, non-adhesive contact between randomly rough surfaces.

The contact mechanics model used above is based on continuum mechanics, and the only information related to the adhesive interaction between the surfaces is the interfacial binding energy (per unit area) γ for flat surfaces. In reality, the interaction between two solids depends on the (atom–atom) interaction potential across the two surfaces, and at least one more parameter, a length a of the order of an atomic distance, is necessary in order to fully characterize the interaction between the surfaces at the atomistic level. This is well known in the context of the adhesive contact between a spherical asperity (with a radius R) and a flat surface, where different models such as the JKR [8] or DMT [9] models (and numerical calculations using atomistic models) have been used to describe the contact between solids with different elastic (and adhesive) properties, and different tip radius R. However, for the question which we have addressed above, namely the

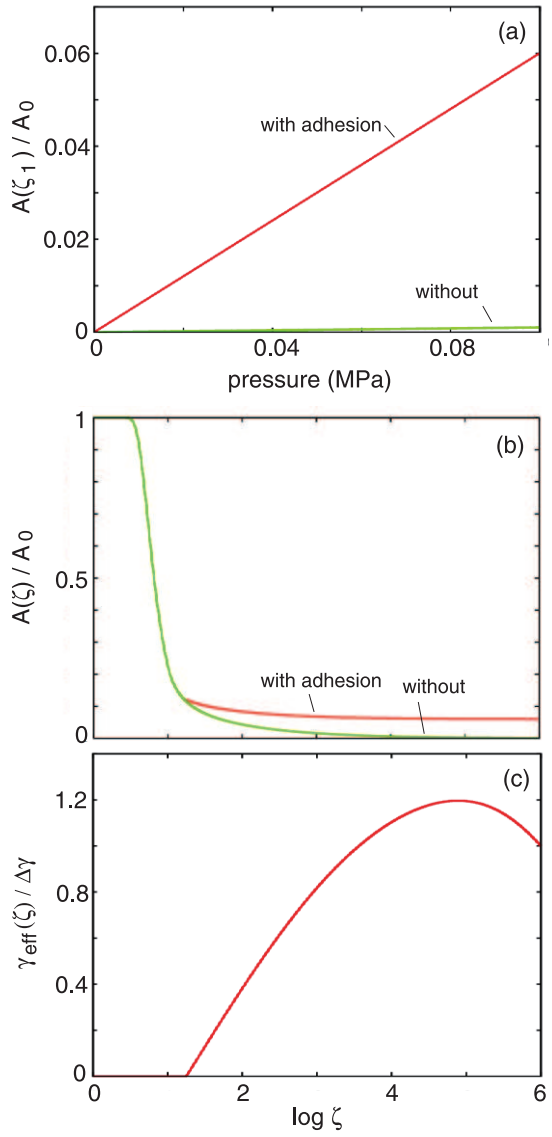

Figure 5. (a) The area of real contact A (in units of the nominal contact area A_0) at the highest magnification $\zeta_1 (=10^6)$ as a function of the nominal squeezing pressure. (b) The area of real contact $A(\zeta)$ (for the pressure $p = 0.1$ MPa) and (c) the effective interfacial binding energy (per unit surface area) (in units of $\Delta\gamma = \gamma_1 + \gamma_2 - \gamma_{12}$) as a function of the logarithm (with 10 as the base) of the magnification ζ. Results are shown both with and without adhesion. For the elastic modulus $E = 120$ MPa and the surface with the power spectrum shown in figure 1 with the Hurst exponent $H = 0.6$.

load dependence of the friction coefficient, the nature of the contact at the atomistic level is, in most cases, unimportant for the following reasons: first, note that for an asperity (radius R) in contact with a flat surface, the nature of the adhesive contact can be characterized by the Tabor number [10]

$$\Gamma = \left(\frac{R\gamma^2}{E^2 a^3}\right)^{1/3}.$$

When $\Gamma \gg 1$ the JKR limit is obtained while the DMT limit is obtained for $\Gamma \ll 1$. For $\Gamma \gg 1$ (JKR limit) the contact mechanics does not depend on the length parameter

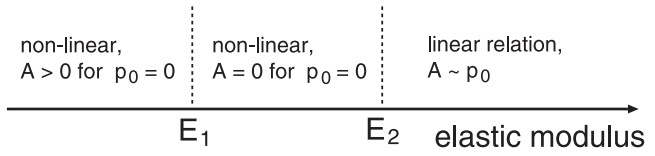

Figure 6. Relation between the area of real contact $A(\zeta_1)$ and the squeezing pressure p_0 as a function of the elastic modulus (schematic).

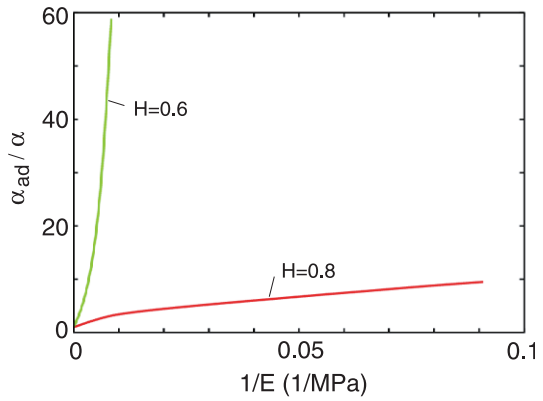

Figure 7. The ratio α_{ad}/α between the slopes of the relation between the contact area A and the applied normal force F_N with the adhesional interaction included (α_{ad}) and without the adhesional interaction (α). The adhesional interaction is characterized by the interfacial binding energy (per unit area) $\Delta\gamma = \gamma_1 + \gamma_2 - \gamma_{12} = 0.05$ J m^{-2}. For self-affine fractal surfaces (with the Hurst exponent $H = 0.6$ and 0.8) with the power spectra shown in figure 1.

a characterizing the wall–wall interaction potential, but it depends only on the work of adhesion γ. However, for $\Gamma < 5$, the adhesive bond depends also on the bond length parameter a (and on the detailed form of the interaction potential). Now, let us consider a rough surface at the magnification ζ. At this magnification we observe asperities with the typical curvature $1/R \approx h_{rms}(\zeta)q^2$, where $q = q_0\zeta$ and where $h_{rms}(\zeta)$ is the root-mean-square roughness due to the surface roughness with wavelength below $2\pi/q$. For a self-affine fractal surface we have $h_{rms}(\zeta) \approx h^0_{rms}\zeta^{-H}$, where $h^0_{rms} = h_{rms}(1)$ is the macroscopic rms roughness amplitude. Thus, at the magnification ζ:

$$\Gamma(\zeta) = \left(\frac{\gamma^2\zeta^{H-2}}{E^2 q_0^2 h^0_{rms} a^3}\right)^{1/3} \sim \zeta^{(H-2)/3}.$$

Since for a self-affine fractal surface $0 \leqslant H \leqslant 1$, $\Gamma(\zeta)$ increases with decreasing magnification, and typically $\Gamma(\zeta) \gg 1$ before reaching the macroscopic length scale. Thus, at low enough resolution the detailed form of the wall–wall interaction potential can usually be neglected.

When the *macroscopic* interfacial binding energy (per unit area), γ_{eff}, is non-vanishing it is necessary to take into account the macroscopic shape of the object as this influences the nominal contact area A_0. The most well-defined configuration (used in most model studies) consists of an elastic sphere in contact with a nominally flat substrate. If the effective elastic

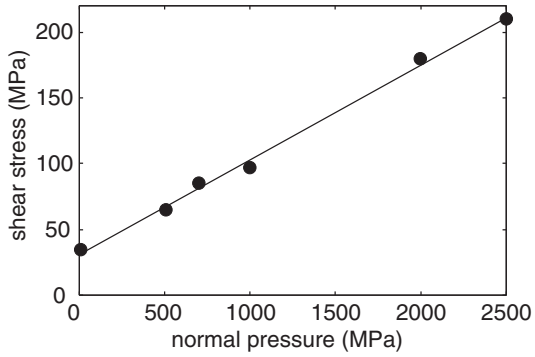

Figure 8. The relation, after 200 nm run-in distance, between the frictional shear stress and the normal pressure for $C_{100}H_{202}$ polymer slab sliding on $C_{100}H_{202}$ polymer slab. Sliding velocity $v = 10$ m s^{-1}, and background temperature $T = 300$ K. The solid line is a linear fit to the data $\sigma_f = \sigma_c + \beta p_0$ with $\sigma_c = 31.5$ MPa and $\beta = 0.07$.

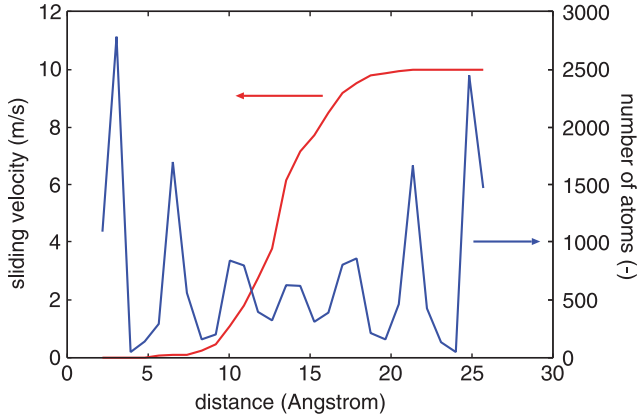

Figure 9. The velocity profile and the number density of bead units as a function of the distance between the two solid walls. For $C_{100}H_{202}$ polymer slab sliding at the sliding velocity $v = 10$ m s^{-1}, background temperature $T = 300$ K and normal pressure $p = 10$ MPa. Note the strong layering and that most of the slip occurs between the most central layer of lubricant molecules and the two nearby layers.

modulus is not too high the contact mechanics can be described with the JKR theory [8]. The nominal contact region will be a circular region with the radius

$$r_0 = \left(\frac{R}{E^*}\right)^{1/3} \left(F_a^{1/2} + (F_N + F_a)^{1/2}\right)^{2/3} \tag{1}$$

where $E^* = E/(1-\nu^2)$ and where the pull-off force

$$F_a = \tfrac{3}{2}\pi R \gamma_{\rm eff}. \tag{2}$$

In this equation $\gamma_{\rm eff} = \gamma_{\rm eff}(L/r_0)$ is the (macroscopic) effective interfacial binding energy (per unit area) for the case when only surface roughness components of wavelength $\lambda < r_0$ are included when calculating $\gamma_{\rm eff}$. Thus, $\gamma_{\rm eff}(L/r_0)$ will depend on the radius r_0 and equation (1) must be solved self-consistently together with the expression for $\gamma_{\rm eff}(\zeta)$ given by the contact mechanics theory described above. The solution to these equations gives the radius r_0 of the contact region and the macroscopic interfacial binding energy (per unit area) $\gamma_{\rm eff}$.

3. Dependence of the frictional shear stress σ_f on the pressure p

As stated earlier, the relation $F_f \propto F_N$ usually holds independent of the detailed dependence of the frictional shear stress $\sigma_f(p)$ on the local (squeezing) pressure $p(\mathbf{x})$. However, this is only true as long as the area of real contact depends linearly on the load. For elastically soft solids (e.g. rubber or gelatin), or for hard solids with extremely smooth surfaces, nearly complete contact may occur in the nominal contact region, and in this case Amonton's law may no longer hold. If $A = A_0$ the friction force F_f will depend on the pressure distribution in the contact area and we may write

$$F_f = \int_{A_0} {\rm d}^2x\ \sigma_f(p(\mathbf{x})).$$

In particular, if σ_f can be considered as pressure-independent, then the friction force $F_f = \sigma_f A_0$. This expression may still depend on the normal load F_N since the nominal contact area A_0 will, in general, increase with increasing load, but usually not linearly so that Amonton's law will not hold in this case.

Here we will briefly discuss the pressure dependence of σ_f for polymers sliding on polymers. For a more detailed study, see [11].

Figure 8 shows the relation, after a 200 nm run-in distance, between the frictional shear stress, σ_f, and the normal pressure, p_0, for a ∼3 nm thick $C_{100}H_{202}$ polymer slab confined between two flat 'metal' surfaces, when the polymer–metal bond is so strong that no slip occurs at the polymer–metal interfaces. The solid line is a linear fit to the data $\sigma_f = \sigma_c + \beta p_0$ with $\sigma_c = 31.5$ MPa and $\beta = 0.07$. The sliding velocity $v = 10$ m s^{-1}, but even at this relatively high sliding velocity the frictional energy dissipation in the polymer film gives rise to negligible temperature increase. The reason for this is that the polymer film is very thin, and that the wall atoms are coupled to a thermostat (at temperature $T = 300$ K) so that the excess (friction-induced) thermal energy is effectively removed from the system, leading to the negligible temperature increase. We have also performed calculations for the sliding velocity $v = 1$ m s^{-1} but the results are nearly the same as for $v = 10$ m s^{-1}. The value for β found above is very similar to the value found by Rottler and Robbins [12] for the pressure dependence of the yield stress and the friction of models of glassy atomic solids and glassy polymer solids.

That the slip occurs inside the polymer film, rather than at the polymer–metal interfaces, is illustrated in figure 9 which shows the velocity profile and the number density of bead units as a function of the distance between the two solid walls. Note the strong layering and that most of the slip occurs between the most central layer of lubricant molecules and the two nearby layers.

The results presented above for polymer sliding on polymer is in good agreement with experimental data. Thus, Whitten *et al* [13] have studied the shear stress when a spherical glass indenter is sliding on different types of

polymers. It is likely that polymer molecules will be transferred to the glass surface so that the sliding interface will be polymer against polymer. The experimental data for the frictional shear stress σ_f as a function of the normal stress or pressure p_0 was fitted to a linear relation

$$\sigma_f = \sigma_c + \beta p_0. \tag{3}$$

For four different polymers (poly(methyl methacrylate) (PMMA), polystyrene (PS), poly(phenylene oxide) (PPO) and polycarbonate (PC)) it was found that $\sigma_c = 39$, 25, 20 and 17 MPa (average 25 MPa) while the parameter $\beta = 0.10$, 0.13, 0.05 and 0.06 (average 0.09). For the C_{100} system we find $\sigma_c = 31.5$ MPa and $\beta = 0.07$ which are similar to the experimental results.

The basic physics behind the pressure dependence of the frictional shear stress can be understood as follows [14]. During slip the separation between the atoms or molecules at the sliding interface increases by a small amount Δh. This expansion makes work against the applied pressure p_0 given by $f\Delta h = p_0 a^2 \Delta h$ where a is the block adsorbate constant. In addition, the binding energy will decrease in the on-top position because of the reduced number of nearest-neighbor substrate atoms (or molecules). If we denote this energy difference by $\epsilon_0 > 0$ we get the energy difference (per unit block atom or molecule)

$$\Delta E = \epsilon_0 + p_0 a^2 \Delta h.$$

If this increase in energy between on-top and bridge positions is fully lost into heat during the slip downhill from the on-top to the bridge position, then

$$\sigma_f a^2 b = \Delta E$$

where b is the substrate constant, giving

$$\sigma_f = \frac{\epsilon_0}{a^2 b} + \frac{\Delta h}{b} p_0$$

or

$$\sigma_f = \sigma_c + \beta p_0 = \beta(p_{ad} + p_0) \tag{4}$$

with $\sigma_c = \epsilon_0/(a^2 b)$, $p_{ad} = \epsilon_0/(a^2 \Delta h)$ and $\beta = \Delta h/b$.

Note that even if the frictional stress depends linearly on the pressure $\sigma_f = \sigma_c + \beta p_0$ the friction force

$$F_f = \sigma_c A_0 + \beta p_0 A_0 = \sigma_c A_0 + \beta F_N$$

will, in general, depend nonlinearly on the load because the area of real contact A_0 will usually depend nonlinearly on the load, e.g. for a spherical lens against a flat it will be given by the JKR theory (see equation (1)).

In the analytical calculation presented above we have neglected the influence of temperature (or thermal fluctuations) on the process of going over the barrier. That is, it was assumed that the external applied tangential force (or stress) alone pulls the system over the lateral pinning barriers, and that this happens everywhere simultaneously. At the high sliding velocities used in our MD simulation, the thermal effect should be rather unimportant. However, for small sliding velocities, thermal fluctuations will be very important. In this case slip will not occur everywhere simultaneously, but small nanometer-sized interfacial regions of linear size D will be individually pinned and perform stress-aided thermally induced jumps from one pinned state to another (local interfacial rearrangement processes). (Note that thermal effects can only become important for small (nanometer-sized D) regions, since simultaneous going-over-the-barrier everywhere requires infinitely large energy for an infinite system, except, perhaps for an incommensurate interface.) This process has been studied in detail both theoretically and experimentally [15–20].

4. Sliding-induced reduction in adhesion

As shown in section 2, surface roughness can strongly reduce the adhesion between solids, even if the roughness is so small that (nearly) complete contact occurs in the nominal contact area. The reason for this is that, for rough surfaces, the surfaces of the solids must bend at the interface in order to make atomic contact. This deformation results in elastic energy stored at the interface, which is (partly) given back during pull-off, resulting in a strong roughness-induced reduction in the pull-off force.

Recent experiments performed with solids with perfectly smooth surfaces indicate that sliding motion may also reduce the (macroscopic) adhesive interaction between solids. In the experiments a silicon rubber (PDMS) lens was slid on a perfectly smooth silicon wafer surface covered by inert grafted monolayer films [21, 22]. In stationary contact, the contact area was enhanced because of the adhesional interaction, with the radius of the circular contact region given by JKR theory (see equation (1)). During sliding the contact area gradually decreased with increasing sliding velocity, and at the sliding velocity where the frictional shear stress was maximal ($v \approx 1$ cm s^{-1}), the radius of the contact area was equal to that predicted by the Hertz (non-adhesive) contact theory. Two explanations for this phenomena have been suggested.

Wu-Bavouzet *et al* [22] have suggested that, during sliding at high enough velocity, almost all the adhesive bonds between the rubber and the substrate are broken. However, the measured work of adhesion (about 0.04 J m^{-2}) is consistent with the weak van der Waals interaction, which is rather long ranged (the interaction energy per unit surface area between the surfaces falls of as $1/d^2$ with the separation d between the surfaces) and since the equilibrium separation is of the order of $d \approx 4$ Å the separation must increase with at least a nanometer for the wall–wall interaction to become negligible. But in this case the sliding friction force should be very small. However, the experiment indicates a maximum in the frictional shear stress when $v \approx 1$ cm s^{-1}, when the contact is already Hertzian-like. Thus, it is very unlikely that breaking adhesive bonds is the origin of the observed transition from JKR (adhesive) contact to Hertz (non-adhesive) contact.

A second possible origin of the reduction in adhesion at high enough sliding velocity is related to the build up of elastic deformation energy, due to the frictional shear stress at the sliding interface, which may affect the adhesional interaction in a very similar way as surface roughness. Thus, during sliding elastic energy is 'stored' at the interface, which helps

to break the adhesive bonds, making the contact essentially non-adhesive at high enough sliding velocity. There are two types of elastic energy induced by the friction: one in a thin (nanometer-thick) layer close to the sliding interface and one associated with the macroscopic shear stress which extends into the rubber lens a distance of the order of the radius of the contact area.

Let us consider the first source of elastic energy. When a rubber lens is sliding on a flat substrate small regions (stress domains) of linear size D will perform 'jumps' between pinned states. This will result in elastic energy stored at the interface. Neglecting temperature effects the average elastic energy stored in one stress domain will be of the order of $kx^2/2$ where the effective spring constant $k \approx DE$ (where E is the absolute value of the rubber elastic modulus at the frequency associated with the stick–slip motion of the stress domain) and where the displacement x is given by $kx \approx \sigma_p D^2$ where σ_p is the depinning stress. Thus the elastic energy stored per unit area is $\gamma^* = (\sigma_p D^2)^2/(2kD^2) = \sigma_p^2 D/(2E)$. In a typical case $D \approx 30$ nm, $\sigma_p \approx 1$ MPa and $E \approx 10$ MPa giving $\gamma^* \approx 0.001$ J m^{-2}, which is completely negligible compared to the interfacial binding energy $\Delta\gamma \approx 0.05$ J m^{-2}. Taking into account thermal effects will make γ^* even smaller. Thus this source of elastic energy will have a negligible influence on the macroscopic contact radius.

Let us now consider the influence of the macroscopic frictional shear stress at the sliding interface on the reduction in contact area. This mechanism has already been studied by Savkoor *et al* [23]. The total energy

$$U = E^* \left(h^2 r_0 - \frac{2}{3}\frac{h r_0^3}{R} + \frac{1}{5}\frac{r_0^5}{R^2} \right) - \pi r_0^2 \Delta\gamma + U_1. \quad (5)$$

The first and second terms in this expression represent the elastic energy [30, 31] due to the vertical deformations of the ball, and the adhesional binding energy at the ball–substrate interface, respectively. The last term U_1 is the elastic energy arising from the shear deformations of the ball. It is shown in appendix B that

$$U_1 = \alpha E^* \delta^2 r_0 \quad (6)$$

where δ is the displacement (of the center of mass) of the contact area due to the tangential force $F_\parallel = \sigma_f \pi r_0^2$. Thus we get

$$F_N = \frac{\partial U}{\partial h} = E^* \left(2hr_0 - \frac{2}{3}\frac{r_0^3}{R} \right), \quad (7)$$

$$F_\parallel = \frac{\partial U}{\partial \delta} = 2\alpha E^* r_0 \delta. \quad (8)$$

Note that F_N is negative during pull-off (where $h < 0$). The contact radius r_0 is obtained by minimizing U with respect to the radius r_0 which gives

$$\frac{\partial U}{\partial r_0} = E^* \left(h^2 - 2\frac{h r_0^2}{R} + \frac{r_0^4}{R^2} \right) - 2\pi r_0 \Delta\gamma + \alpha E^* \delta^2 = 0. \quad (9)$$

Using (7)–(9) gives after some simplifications

$$r_0^3 = \frac{3R}{4E^*} \left(2F_a + F_N + 2\left[F_a F_N + F_a^2 - \frac{1}{4\alpha} F_\parallel^2 \right]^{1/2} \right) \quad (10)$$

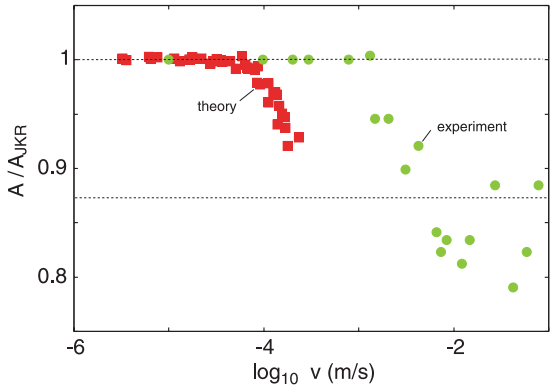

Figure 10. The ratio of the contact areas during sliding and in stationary contact as a function of velocity for PDMS ($E = 4.8$ MPa, $\Delta\gamma = 0.042$ J m^{-2}) against a self-assembled monolayer. As the sliding velocity increases, the contact area drops from the JKR prediction (upper dashed line) to the Hertzian prediction (lower dashed line). The circle and square data points are the measured and calculated (using equation (13)) results, respectively. The normal load $F_N = 0.048$ N. Experimental data from [21].

where $F_a = 3\pi R \Delta\gamma/2$. Equation (10) is only valid as long as the term in the $[\cdots]$ is non-negative, i.e. until

$$F_\parallel = 2\sqrt{\alpha} \left(F_a F_N + F_a^2 \right)^{1/2}. \quad (11)$$

In the experiment by Vorvolakos *et al* [21], $F_N = 0.048$ N and using $R = 0.25$ cm and $\Delta\gamma = 0.042$ J m^{-2} gives $F_a \approx 5.0 \times 10^{-4}$ N.

When $F_a = F_\parallel = 0$ we have the Hertz contact limiting case where the radius of the contact area

$$r_H^3 = \frac{3RF_N}{4E^*}. \quad (12)$$

For the parameters given above we get $r_H \approx 2.4 \times 10^{-4}$ m. Using (12) we can therefore write (10) as

$$\left(\frac{r_0}{r_H} \right)^3 = 1 + 2\frac{F_a}{F_N} + 2\left[\frac{F_a}{F_N} + \left(\frac{F_a}{F_N} \right)^2 - \frac{1}{4\alpha} \left(\frac{F_\parallel}{F_N} \right)^2 \right]^{1/2}. \quad (13)$$

At low sliding velocities, where $F_\parallel \approx 0$, we obtain the JKR contact radius

$$\left(\frac{r_{JKR}}{r_H} \right)^3 = 1 + 2\frac{F_a}{F_N} + 2\left[\frac{F_a}{F_N} + \left(\frac{F_a}{F_N} \right)^2 \right]^{1/2} \approx 1 + 2\left(\frac{F_a}{F_N} \right)^{1/2} \quad (14)$$

where we have used that in the present case $F_a/F_N \ll 1$. The contact radius r_c at the limit when (11) is obeyed is given by

$$\left(\frac{r_c}{r_H} \right)^3 = 1 + 2\frac{F_a}{F_N}.$$

Note that in our case $r_{JKR} \approx 1.07 r_H$ while $r_c \approx 1.007 r_H$, i.e. when the velocity has increased to the point where the friction force $F_\parallel$ obeys (11), then the contact radius is nearly at its Hertzian value. In figure 10 we show the calculated

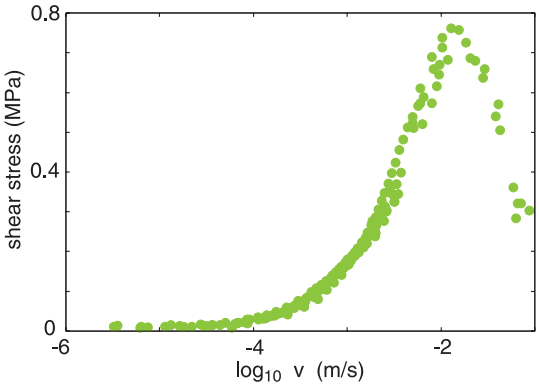

Figure 11. The measured frictional shear stress as a function of velocity for PDMS ($E = 4.8$ MPa, $\Delta\gamma = 0.042$ J m^{-2}) against a self-assembled monolayer. The normal load $F_N = 0.048$ N. Based on experimental data from [21].

(from (13) and (14)) ratio A/A_{JKR} as a function of the sliding velocity. In the calculation we have assumed that the frictional shear stress is constant in the ball–substrate contact area which gives $\alpha \approx 0.67$ (see appendix B). The lower dashed line in figure 10 is given by $A/A_{JKR} = A_H/A_{JKR} \approx 0.87$. In the calculation we have used the measured friction force $F_\parallel$ (see figure 11). Note that the theory prediction does not agree with the experimental data. We believe that the reason for this is that the frictional shear stress is not constant in the contact area as assumed above, but reduced in the region where the normal stress is tensile. The basic idea is that the rubber at the sliding interface can be in two different states with nearly the same adhesive binding to the substrate, but where the rubber experiences very different pinning potentials. Thus, in one state the rubber molecules at the interface can rearrange or adjust to the corrugated substrate potential to give a state with 'strong' interfacial pinning potential. In the other state, due to the influence of the tensile stress, the molecules are stretched in the normal direction and are not able to adjust as well to the corrugated substrate potential, resulting in a weaker pinning potential and, during slip, a smaller shear stress. We assume that, in a circular strip at the boundary of the contact region, where the normal stress is tensile, the rubber is in the second state. In this case the elastic energy release rate, as the contact radius decreases (from the JKR limit), will be smaller, and it is necessary to go to higher slip velocities (where the frictional shear stress is likely to be larger), in order for the contribution to the energy release rate from the elastic energy stored in the shear deformation to be so large as to reduce the contact radius.

5. Summary and conclusion

In this paper we have discussed how the area of real contact A depends on the load or normal force F_N as two elastic solids with randomly rough surfaces are squeezed together. We have shown that, even when the adhesive interaction between the solids is taken into account, one expects in most cases that $A \propto F_N$ and the pressure distribution in the contact regions is independent of the load. We believe that this is the explanation for why the friction force is proportional to the load in most cases (Amonton's friction law).

For very smooth surfaces or for elastically soft solids such as rubber or gelatin, the area of real contact may approach the nominal contact area. In this case the friction force will depend on the detailed pressure dependence of the frictional shear stress σ_f. We have performed extensive MD calculations for metal–polymer and polymer–polymer sliding interfaces and always found a nearly linear dependence of σ_f on the squeezing pressure p_0: $\sigma_f = \beta(p_{ad} + p_0)$ where the adhesional pressure p_{ad} depends on the energetic and geometrical corrugation of the atomic (or molecular) layers at the interface where the slip occurs. Typically $p_{ad} \approx 1$ GPa so that σ_f will depend on the pressure p_0 essentially only for squeezing pressures of the order of 100 MPa or more. The friction force $F_f = A_0\sigma_f = A_0\beta(p_{ad} + p_0) = \beta(A_0 p_{ad} + F_N)$ will, in general, depend nonlinearly on the load because the nominal contact area A_0 will, in most cases, increase nonlinearly with the load, e.g. it is given by the JKR theory when an elastic lens is squeezed against a flat. Thus, when the adhesion is so strong as to result in nearly complete contact in the apparent contact area, the friction force will depend nonlinearly on the load and Amonton's friction law will not hold.

During sliding deformation energy, due to the frictional shear stress, will be stored in the asperity contact regions. This may result in a decrease in the adhesive contact area: reducing the contact area results in a reduced adhesive bonding energy $A\Delta\gamma$, but this is compensated by a reduction in the stored elastic energy. That is, the contact area is determined by minimizing the total energy and since the elastic energy increases during slip because of the shear deformations of the solids in the vicinity of the contact regions, the contact area will change in such a way as to minimize the total energy (elastic plus adhesive energies). Since the elastic energy in an asperity contact region is stored in the volume element $\sim d^3$ (where d is the linear size of the contact region) and the interfacial binding energy is proportional to the contact area $\sim d^2$, one expects that, as the frictional shear stress increases, the contact area will decrease towards the non-adhesive limit, as indeed found by Vorvolakos and Chaudhury [21] (see section 4) for a lens in contact with a flat. This will, of course, also influence the friction force.

Acknowledgments

BP performed part of this work while visiting ORNL. This work was supported in part by Oak Ridge National Laboratory, managed by UT-Battelle, LLC, for the US Department of Energy under contract no. DE-AC05-00OR22725. We thank M K Chaudhury for supplying the experimental data for figure 11. IMS and VNS acknowledge support from IFF, FZ-Jülich, hospitality and help of the staff during their research visits.

Appendix A

Asperity contact theories, such as the Greenwood–Williamson [24] theory and the theory of Bush *et al* [25], are often used to motivate that for randomly rough surfaces the area of real contact A depends linearly on the load F_N. However, for

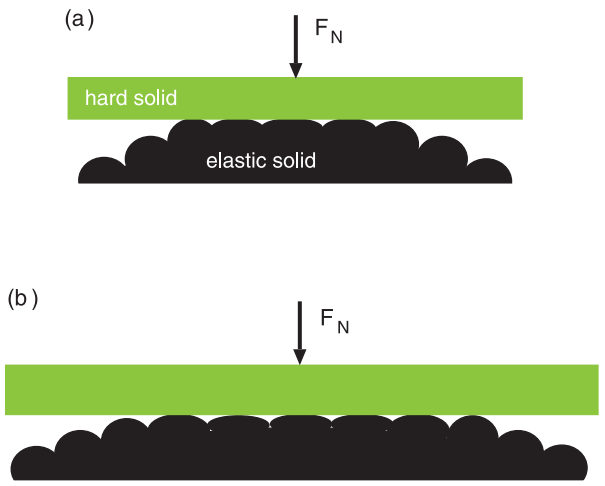

Figure A.1. A rigid solid with a flat surface squeezed against an elastic solid with roughness on two length scales: small bumps on large bumps. In (a) it is assumed that only the small bumps undergo elastic deformation while in (b) both the small bumps and the large bump undergo elastic deformation. In asperity contact theories it is usually assumed that only the smallest bumps undergo elastic deformation. The correct picture, where bumps on all length scales can deform elastically, gives drastically different contact mechanics when roughness occurs on many different length scales.

surfaces with roughness over many different length scales, as is almost always the case in real systems, these theories predict that the linear relation between A and F_N holds over an extremely small range of squeezing forces. However, numerical simulations have shown that A and F_N are linearly related until the contact area becomes of the order of 10% of the nominal contact area A_0. Thus, the asperity contact models mentioned above fail qualitatively in most cases of practical interest. In particular, these theories cannot be used to explain (assuming purely elastic deformations) why the friction force usually is proportional to the load (Amonton's friction law).

That asperity contact theories fail to predict that the area of real contact is proportional to the load for a physically meaningful range of loads has recently been demonstrated by detailed calculations presented by Carbone *et al* [26]. The basic physics is easy to understand. Randomly rough surfaces with roughness on many different length scales have roughness of the type 'bumps-on-top-of-bumps-on-top-of-bumps-$\cdots$'. In figure A.1 we illustrate this with a surface with roughness on two length scales consisting of small bumps on top of large bumps (only one large bump is shown in the figure). In the asperity contact models it is assumed that only the smallest bumps deform elastically as in figure A.1(a). However, in reality the small bumps will exert a force on the big bumps which also will deform as in A.1(b). This will result in more small bumps being in contact with the upper surface and a larger contact area and, more important, a contact area which increases linearly with the squeezing force until the area of real contact reaches $\sim$10% of the nominal contact area. On the contrary, for surfaces with roughness on many different length scales, the asperity contact models fail to predict a linear relation between A and F_N already for extremely small contact area. In particular, if surface roughness occurs the whole way down to the nanoscale, then the largest physical compression of the two surfaces will be of the order of a nanometer (which will flatten out the nanobump which first comes into contact with the (flat) bottom surface of the block) and the area of real contact at this point will be extremely small. It is this very same effect which gives rise to a qualitatively wrong relation between the (average) interfacial separation $\bar{u}$ and the load [27]: for asperity contact models $p \sim \exp(-b\bar{u}^2)$ while the exact result (for large separation) is exponential, $p \sim \exp(-a\bar{u})$.

The contact mechanics model of Persson [28] includes the elastic coupling between the asperities and predicts, in accordance with numerical studies, that the contact area varies linearly with the load until A becomes of the order of 10% of the nominal contact area; see figure 10 in [29] for an example.

Appendix B

Assume that a constant shear stress $\sigma_\parallel$ acts in the x direction on the surface of a semi-infinite elastic solid within the circular region $r < r_0$ and area $A_0 = \pi r_0^2$. This will result in a surface displacement field $\mathbf{u}(\mathbf{x})$. We define the center-of-mass displacement

$$u_\parallel = \frac{1}{A_0}\int_{A_0} \mathrm{d}^2x\; u_x(\mathbf{x}).$$

The total shear force $F_\parallel = A_0\sigma_\parallel$. We define the spring constant $k_\parallel$ so that

$$k_\parallel u_\parallel = F_\parallel.$$

Using the theory of elasticity we get [30]

$$u_x(\mathbf{x}) = \frac{1}{2\pi G}\int_{A_0} \mathrm{d}^2x'\;\sigma_\parallel\left(\frac{1-\nu}{|\mathbf{x}-\mathbf{x}'|} + \frac{\nu(x-x')^2}{|\mathbf{x}-\mathbf{x}'|^3}\right)$$

and

$$u_\parallel = \frac{1}{2\pi G}\frac{1}{A_0}\sigma_\parallel\int_{A_0} \mathrm{d}^2x\,\mathrm{d}^2x'\left(\frac{1-\nu}{|\mathbf{x}-\mathbf{x}'|} + \frac{\nu(x-x')^2}{|\mathbf{x}-\mathbf{x}'|^3}\right)$$

where G is the shear modulus and ν the Poisson ratio. We introduce polar coordinates and write $x = r_0\xi\cos\phi$, $y = r_0\xi\sin\phi$ and similar for $\mathbf{x}'$. We get

$$u_\parallel = \frac{1}{2\pi G}\frac{1}{A_0}\sigma_\parallel r_0^3\int_0^1 \mathrm{d}\xi\,\mathrm{d}\xi'\xi\xi'\int_0^{2\pi}\mathrm{d}\phi\,\mathrm{d}\phi' \times\left(\frac{1-\nu}{s} + \frac{\nu(\xi\cos\phi-\xi'\cos\phi')^2}{s^3}\right) \tag{B.1}$$

where

$$s = \left[(\xi\cos\phi-\xi'\cos\phi')^2 + (\xi\sin\phi-\xi'\sin\phi')^2\right]^{1/2}.$$

The integrals in (B.1) can easily be performed numerically and using that $G = E/(2(1+\nu)) = E^*(1-\nu)/2$ we can write

$$u_\parallel = \frac{1}{r_0E^*}\frac{A+B\nu}{1-\nu}F_\parallel$$

where $A \approx 0.55$ and $B \approx -0.28$. Thus

$$k = r_0 E^* \frac{1-\nu}{A + B\nu}. \tag{B.2}$$

It is interesting to note that, if instead of a constant shear stress within the area A_0, one assumes a constant displacement (which requires a tangential stress $\sim [1 - (r/r_0)^2]^{-1/2}$), then the spring constant [30]

$$k = r_0 E^* \frac{4(1-\nu)}{2-\nu}. \tag{B.3}$$

For rubber ($\nu \approx 0.5$) we get $k \approx 1.22 r_0 E^*$ and $k \approx 1.33 r_0 E^*$ from (B.2) and (B.3), respectively. The stored elastic energy when $u_\parallel = \delta$ is

$$U_1 = \tfrac{1}{2} k \delta^2 = \alpha E^* \delta^2 r_0$$

with

$$\alpha = \frac{1-\nu}{2(A + B\nu)}.$$

For rubber $\nu \approx 0.5$ giving $\alpha \approx 0.67$.

References

[1] Persson B N J 2000 *Sliding Friction: Physical Principles and Applications* 2nd edn (Heidelberg: Springer)
[2] Dowson D 1979 *History of Tribology* (New York: Longman)
[3] Bowden F P and Tabor D 1958 *The Friction and Lubrication of Solids* (Oxford: Oxford University Press)
[4] Persson B N J, Albohr O, Mancosu F, Peveri V, Samoilov V N and Sivebaek I M 2003 *Wear* **254** 835
[5] Klüppel M and Heinrich G 2000 *Rubber Chem. Technol.* **73** 578
Le Gal A and Klüppel M 2008 *J. Phys.: Condens. Matter* **20** 015007
[6] He G, Müser M H and Robbins M O 1999 *Science* **284** 1650
[7] Persson B N J 2002 *Eur. Phys. J.* E **8** 385
[8] Johnson K L, Kendall K and Roberts A D 1971 *Proc. R. Soc.* A **324** 301
[9] Derjaguin B V, Muller V M and Toporov Y P 1975 *J. Colloid Interface Sci.* **53** 314
[10] Tabor D 1977 *J. Colloid Interface Sci.* **58** 2
[11] Sivebaek I M, Samoilov V N and Persson B N J 2008 *Eur. Phys. J.* E **27** 37
[12] Rottler J and Robbins M O 2005 *Comput. Phys. Commun.* **169** 177
[13] Whitten P G and Brown H R 2007 *Phys. Rev.* E **76** 026101
[14] See, e.g. Israelachvili J N 1992 *Fundamentals of Friction: Macroscopic and Microscopic Processes* (*NATO ASI Series E: Applied Sciences* vol 220) ed I L Singer and H M Pollock (Dordrecht: Kluwer–Academic)
[15] Persson B N J 1995 *Phys. Rev.* B **51** 133568
[16] Briscoe B J 1992 *Fundamentals of Friction: Macroscopic and Microscopic Processes* (*NATO ASI Series E: Applied Sciences* vol 220) ed I L Singer and H M Pollock (Dordrecht: Kluwer–Academic)
[17] Schallamach A 1963 *Wear* **6** 375
[18] Persson B N J and Volokitin A I 2006 *Eur. Phys. J.* E **21** 69
[19] Drummond C, Israelachvili J and Richetti P 2003 *Phys. Rev.* E **67** 066110
Drummond C, Elezgaray J and Richetti P 2002 *Europhys. Lett.* **58** 503
[20] Baumberger T and Caroli C 2006 *Adv. Phys.* **55** 279
Baumberger T, Caroli C and Ronsin O 2003 *Eur. Phys. J.* E **11** 85
Ronsin O and Coeyrehourcq K L 2001 *Proc. R. Soc.* A **457** 1277
[21] Vorvolakos K and Chaudhury M K 2003 *Langmuir* **19** 6778
[22] Wu-Bavouzet F, Clain-Burckbuchler J, Buguin A, De Gennes P-G and Brochard-Wyart F 2007 *J. Adhes.* **83** 761
Brochard-Wyart F and de Gennes P-G 2007 *Eur. Phys. J.* E **23** 439
[23] Savkoor A R and Briggs G A D 1977 *Proc. R. Soc.* A **356** 103
Savkoor A R 1992 *Fundamentals of Friction: Macroscopic and Microscopic Processes* (*NATO ASI Series E: Applied Sciences* vol 220) ed I L Singer and H M Pollock (Dordrecht: Kluwer–Academic)
[24] Greenwood J A and Williamson J B P 1966 *Proc. R. Soc.* A **295** 300
[25] Bush A W, Gibson R D and Thomas T R 1975 *Wear* **35** 87
[26] Carbone G and Bottiglione F 2008 *J. Mech. Phys. Solids* **56** 2555
[27] Persson B N J 2007 *Phys. Rev. Lett.* **99** 125502
[28] Persson B N J 2001 *J. Chem. Phys.* **115** 3840
[29] Persson B N J 2006 *Surf. Sci. Rep.* **61** 201
[30] Johnson K L 1985 *Contact Mechanics* (Cambridge: Cambridge University Press)
[31] See also appendix A in Persson B N J and Tosatti E 2001 *J. Chem. Phys.* **115** 5597